Bioorganic & Medicinal Chemistry Letters 24 (2014) 4714–4723

Contents lists available at ScienceDirect

Bioorganic & Medicinal Chemistry Letters

journal homepage: www.elsevier.com/locate/bmcl

Structure based design of novel 6,5 heterobicyclic mitogen-activated protein kinase kinase (MEK) inhibitors leading to the discovery of imidazo[1,5-*a*] pyrazine G-479

Kirk D. Robarge [a,*], Wendy Lee [a], Charles Eigenbrot [b], Mark Ultsch [b], Christian Wiesmann [b], Robert Heald [c], Steve Price [c], Joanne Hewitt [c], Philip Jackson [c], Pascal Savy [c], Brenda Burton [c], Edna F. Choo [d], Jodie Pang [d], Jason Boggs [d], April Yang [d], Xioaye Yang [d], Matthew Baumgardner [d]

[a] *Discovery Chemistry, Genentech Inc., 1 DNA Way, South San Francisco, CA, USA*
[b] *Structural Biology, Genentech Inc., 1 DNA Way, South San Francisco, CA, USA*
[c] *Argenta, Discovery Services Charles River, 8-9 Spire Greene Centre, Harlow, Essex CM19 5TR, United Kingdom*
[d] *Drug Metabolism and Pharmacokinetics, Genentech Inc., 1 DNA Way, South San Francisco, CA, USA*

ARTICLE INFO

Article history:
Received 27 June 2014
Revised 1 August 2014
Accepted 5 August 2014
Available online 15 August 2014

Keywords:
Mitogen-activated protein kinase kinase inhibitors
MEK inhibitors
RAS signaling pathway
Imidazo[1,5-*a*] pyrazine

ABSTRACT

Use of the tools of SBDD including crystallography led to the discovery of novel and potent 6,5 heterobicyclic MEKi's [*J. Med. Chem.* **2012**, *55*, 4594]. The core change from a 5,6 heterobicycle to a 6,5 heterobicycle was driven by the desire for increased structural diversity and aided by the co-crystal structure of **G-925** [*J. Med. Chem.* **2012**, *55*, 4594]. The key design feature was the shift of the attachment of the five-membered heterocyclic ring towards the B ring while maintaining the key hydroxamate and anilino pharamcophoric elements in a remarkably similar position as in **G-925**. From modelling, changing the connection point of the five membered ring heterocycle placed the H-bond accepting nitrogen within a good distance and angle to the Ser212 [*J. Med. Chem.* **2012**, *55*, 4594]. The resulting novel 6,5 benzoisothiazole MEKi **G-155** exhibited improved potency versus aza-benzofurans **G-925** and **G-963** but was a potent inhibitor of cytochrome P450's 2C9 and 2C19. Lowering the log*D* by switching to the more polar imidazo[1,5-*a*] pyridine core significantly diminished 2C9/2C19 inhibition while retaining potency. The

Abbreviations: MAPK/ERK kinase (MEK) signaling cascade, The pathway includes many proteins, including MAPK (mitogen-activated protein kinases, originally called ERK, extracellular signal-regulated kinases), which communicate by adding phosphate groups to a neighboring protein, which acts as an 'on' or 'off' switch. Also known as the RAS-RAF-MEK-ERK mitogen-activated protein kinase signaling pathway; KRAS, GTPase KRas also known as V-Ki-ras2 Kirsten rat sarcoma viral oncogene homolog and KRAS, is a protein that in humans is encoded by the KRAS gene; NRAS, The N-ras oncogene is a member of the Ras gene family and an enzyme that in humans is encoded by the NRAS gene. It was named NRAS for its initial identification in human neuroblastoma cells; HRAS, GTPase HRas also known as transforming protein p21 is an enzyme that in humans is encoded by the HRAS gene. Once bound to guanosine triphosphate, activates a Raf kinase like c-Raf, the next step in the MAPK/ERK signaling cascade; BRAF, BRAF is a human gene that makes a protein called B-Raf. The gene is also referred to as proto-oncogene B-Raf and v-Raf murine sarcoma viral oncogene homolog B, while the protein is more formally known as serine/threonine-protein kinase B-Raf; RAF, proto-oncogene serine/threonine-protein kinase also known as c-RAF; AKT, AKT is also known as protein kinase B(PKB), is a serine/threonine-specific protein kinase that plays a key role in multiple cellular processes such as glucose metabolism, apoptosis, cell proliferation, transcription and cell migration; PI3K, phosphatidylinositol-4,5-bisphosphate 3-kinase are a family of enzymes involved in cellular functions such as cell growth, proliferation, differentiation, motility, survival and intracellular trafficking, which in turn are involved in cancer; MEKi's, MAPK/ERK kinase (MEK) signaling cascade inhibitors. A MEK inhibitor is a chemical or drug that inhibits the mitogen-activated protein kinase kinase enzymes MEK1 and/or MEK2. Allosteric MEK inhibitors described herein inhibit both MEK1 and MEK 2; MEK 1,2 inhibitors, MEK 1,2 inhibitors are synonymous with MEKi's; ATP, adenosine triphosphate is a nucleoside triphosphate used in cells as a coenzyme; H-bond, hydrogen bond; BID, twice daily; QD, once daily; CYP, cytochrome P450; log*D* (measured), distribution-coefficient is the ratio of concentrations of a compound in a mixture of two immiscible phases at equilibrium. These coefficients are a measure of the difference in solubility of the compound in these two phases. Log*D*'s have a pH dependence. Log*D* measurements for MEKi's disclosed herein were performed at pH 7.4; *c*log*D*, calculated log*D* @ pH 7.4; *c*log*P*, calculated partition-coefficient (*c*log*P*) is the calculated ratio of concentrations of a compound in a mixture of two immiscible phases at equilibrium. These coefficients are a measure of the difference in solubility of the compound in these two phases. The *c*log*P* value reflects the overall lipophilicity of a molecule; IV, delivered directly into the vein; PO, by mouth; Mic(H/R/M/D/C), Microsomes H(human)/R(rat)/M(mouse)/D(dog)/C(cyno). Incubation of the MEKi's described herein was conducted with liver microsomes from human(HLM) and pre-clinical species rat(RLM), mouse(MLM), dog(DLM), and cyno(CLM) to assess comparative metabolic stability; PEG 400, polyethylene glycol 400 is a low-molecular-weight grade of polyethylene glycol miscible with water and used as vehicle for dosing rats IV and PO; CLp, In vivo total plasma clearance is defined as the volume of blood or plasma cleared of drug in a unit time. It is related to the volume in which the drug is dissolved and the rate at which it is eliminated; $T_{1/2}$ (h), half life of MEK inhibitor when dosed intravenously; ppb, plasma protein binding; Oral exposure, area under the plasma concentration versus time curve (AUC); %*F*, oral bioavailability which is the dose-corrected area under curve (AUC) after oral dosing divided by AUC intravenous; IV/IV, in vitro/in vivo clearance correlation (CL predicted from rat microsome incubation/versus CL observed after intravenous administration in rat).

* Corresponding author. Tel.: +1 650 225 2320; fax: +1 650 742 4943.
E-mail address: kir@gene.com (K.D. Robarge).

http://dx.doi.org/10.1016/j.bmcl.2014.08.008
0960-894X/

Imidazo[1,5-*a*] pyridine
Structure based drug design (SBDD)
Oncology

imidazo[1,5-*a*] pyridine **G-868** exhibited increased potency versus the starting point for this work (azabenzofuran **G-925**) leading to deprioritization of the azabenzofurans. The 6,5-imidazo[1,5-*a*] pyridine scaffold was further diversified by incorporating a nitrogen at the 7 position to give the imidazo[1,5-*a*] pyrazine scaffold. The introduction of the C7 nitrogen was driven by the desire to improve metabolic stability by blocking metabolism at the C7 and C8 positions (particularly the HLM stability). It was found that improving on **G-868** (later renamed **GDC-0623**) required combining C7 nitrogen with a diol hydroxamate to give **G-479**. **G-479** with polarity distributed throughout the molecule was improved over **G-868** in many aspects.

The MAPK/ERK kinase (MEK) signaling cascade is a key regulator of cellular proliferation, differentiation and survival downstream of RAS activation.[2] Upregulation of this pathway occurs in a large fraction of tumors, frequently owing to oncogenic activating mutations in KRAS, NRAS, HRAS and BRAF.[3] Constitutive activation of the extracellular regulated kinase (ERK) cascade, through oncogenic forms of RAS and mutations in BRAF, has been observed in lung, colon, pancreas, kidney, and ovary primary human tumor samples.[4] Whereas BRAF inhibitors have shown remarkable efficacy against melanomas with BRAF (V600E) mutations, these compounds are not effective against KRAS-mutant tumors owing to inhibitor-mediated priming of wild-type RAF signaling.[5–7] As MEK is a common effector downstream of wild-type and mutant RAF,[8,9] MEK inhibitors have the potential to target all tumors dependent on MAPK pathway signaling.

The RAS-RAF-MEK-ERK mitogen-activated protein kinase signaling pathway has emerged as one of the most promising targets for molecularly targeted antitumor agents. Currently, at least twelve MEK inhibitors are at some stage of clinical evaluation for the treatment of cancer (three others have been discontinued) and one has been approved by the FDA for use as a single agent for melanoma (Mekinist™, aka trametinib or GSK 1120212). Many in the field of targeted therapies believe there is greater potential for MEK inhibitors if they are used in combination with other targeted agents such as BRAF,[10] AKT,[11] PI3K inhibitors[12,13] and immunotherapies.[14] Combination therapy has been suggested to better inhibit the MAPK/ERK kinase pathway and therefore prolong treatment effect. The results of phase 1 and 2 clinical studies utilizing a selective BRAF inhibitor, Tafinlar™ (aka dabrafenib), and the selective MEK inhibitor, trametinib, demonstrated the benefit of a combination approach. It was found that dabrafenib and trametinib could be safely combined at 150 mg BID/2 mg QD with rare dose-limiting side effects. The combination therapy significantly improved progression free survival and patients showed a higher rate of response in comparison to dabrafenib monotherapy.[10] However, despite the benefit demonstrated by the MEK/BRAF combination, resistance still developed in most patients after an average of 9.4 months. The mechanisms of resistance to combined RAF/MEK inhibition remain poorly understood.[15]

MEK 1,2 inhibitors[16] bind to an allosteric binding site proximal to the ATP binding site and as a result are exquisitely selective. These compounds form a tertiary complex with the MEK enzyme and ATP and are ATP noncompetitive.[17,18] The binding site for allosteric MEK inhibitors has been previously described.[1] There are seven structurally related MEK inhibitors in the clinic that all possess an anilino 'B-ring' which occupies a lipophilic pocket formed by Leu118, Ile126, Val127, Ile141, Met143, Phe129, Phe209, and Val211 (Fig. 1). These MEKi's all incorporate a halogen at the para position which is lipophilic and polarizable and capable of engaging the carbonyl of Val127 in a halogen bond. Additionally these ATP noncompetitive MEKi's all have a polar group capable of engaging the terminal phosphate of ATP and Lys97. This polar group is typically a hydroxamate, but other polar functionalities such as an amide, a reverse sulfonamide, or a sulfonyl urea can be utilized. A third binding feature is an H-bond acceptor to Ser212. It has recently been disclosed that certain MEKi's with superior efficacy against KRAS tumors form a strong H-bond interaction with the Ser212 in MEK that is critical for blocking MEK feedback phosphorylation by wild-type RAF.[19] The strength of the Ser212 H-bond interaction and position relative to the aniline and hydroxamate is determined by the 'A-ring' to which these moieties are attached (Fig. 1). It has been proposed that increasing the strength of the Ser212/H-bond acceptor interaction results in greater tolerance in the other pharmacophoric elements. A potent MEK inhibitor requires having all three of these binding interactions in place.

In our search for novel MEK inhibitors, we leveraged key information from the X-ray crystal structure of our previously disclosed 5,6 heterobicyclic azabenzofuran **G-925** to scaffold hop to a new class of 6,5 heterobicyclic MEKi's[1] which, like the 5,6 azabenzofuran, engaged the Ser212 in a monodentate interaction. The scaffold hop from the 6,5 to the 5,6 heterobicyclic scaffold was driven by two factors: (1) increasing the structural diversity and (2) to further our understanding of the influence of the A ring on the placement of the Ser212 H-bond accepting nitrogen and how that impacts potency. Modelling indicated the 6,5 isobenzothiazole **G-155** would be tolerated in the MEK binding pocket with the H-bond accepting nitrogen capable of making a good interaction with Ser212. As shown in Figure 2, the 6,5 heterobicyclic isobenzothiazole **G-155**, while equipotent in the biochemical assay showed increased potency versus its azabenzofuran comparator **G-963** in both cell proliferation assays. Typically for our potent MEKi's, the biochemical assay was not as useful as the 72 h cell proliferation assays for differentiation. The cell proliferation (particularly the HCT116 cell proliferation assay) potency was the decision making potency readout used to differentiate our potent MEKi's and determine their progression.

Although isobenzothiazole **G-155** was potent, progression was halted due to potent 2C9/2C19 CYP inhibition (Table 1). It was reasoned that the CYP 2C9/2C19 inhibition could be reduced by lowering lipophilicity and log*D*. A decision was made to introduce polarity into the core and scaffold hop to 6,5 imidazo[1,5-*a*] pyridines. In addition to lowering the lipophilicity (reflected in the *measured* log*D* @ pH 7.4) versus the isobenzothiazole, the imidazo[1,5-*a*] pyridine core increased the structural diversity of the 6,5 heterobicyclic MEKi's and differentiated the pK_a's (cpK_a's using MOKA1.1.0 for **G-155**/**G-868** = 1.83/4.78) which can effect the strength of the H-bond interaction with Ser212. Both imidazo[1,5-*a*] pyridines **G-868**[20,21] and **G-606**[22] retained cell proliferation potency and exhibited greatly reduced 2C9(warfarin)/2C19 (mephenytoin) inhibition (Table 1). Imidazo[1,5-*a*] pyridines **G-868** and **G-606** did not inhibit cytochrome P450's 3A4 (testosterone/midazolam), 2D6 (dextromethorphan) and 1A2 (phenacetin). With three examples of 6,5 heterobicyclic MEKi's with increased

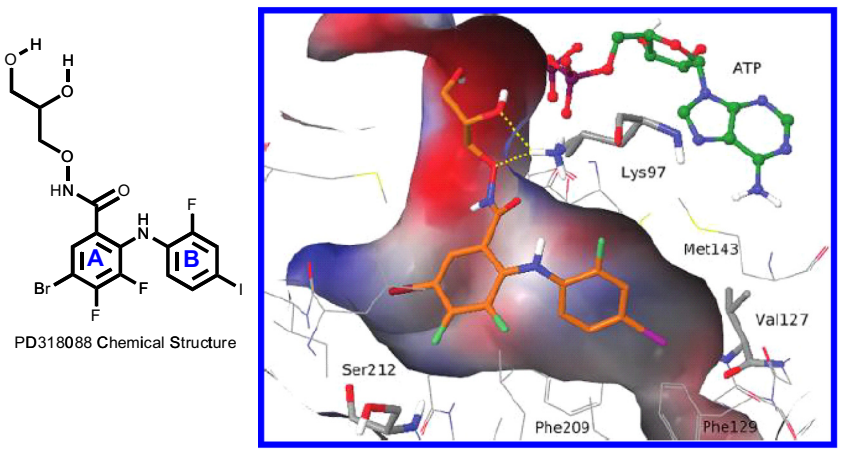

Figure 1. The key interactions of biaryl aniline MEK inhibitors: crystal structure of MEK1 in complex with ATP (green) and **PD318088** (orange) (PDB code 1S9J). Figure 1 adapted with permission from Ref. 1. Copyright 2012 American Chemical Society.

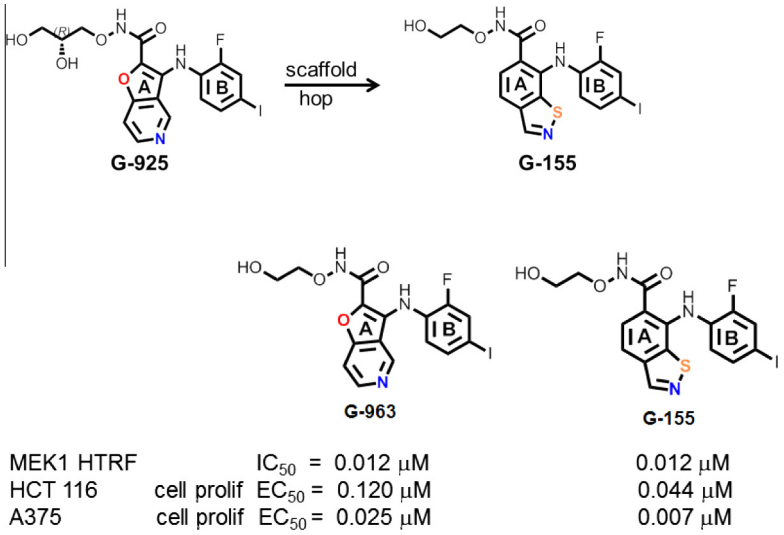

Figure 2. As predicted based on 'fit' to the MEK pharmacophore model, 6,5 heterobicyclic isobenzothiazole **G-155** exhibits increased cell proliferation potency versus its azabenzofuran comparator. HCT116 cell line was derived from malignant human colon cancer cells. A375 cell line was derived from malignant human melanoma cells.

potency versus their direct aza-benzofuran comparator (**G-963**), the 5,6 aza-benzofuran core was deprioritized.

The potency of the 6,5 heterobicyclic MEKi's indicate the positioning of the pharmacophore elements, including the Ser212 H-bond acceptor nitrogen, are well tolerated in the MEK binding pocket. The polar functionality (A-ring dependent) are positioned optimally as shown by the X-ray co-crystal structures in Figure 3.

The imidazopyridine class of MEKi's replaced the benzoisothiazoles with the 5-imidazo[1,5-*a*] pyridines preferred versus the 8-imidazo[1,5-*a*] pyridines. **G-868** was chosen as our new lead. **G-868** exhibited improved predicted metabolic stability in dog and cyno microsomes, low total CL in vivo, longer IV half life, higher AUC and %*F* versus the its direct comparator 8-imidazo[1,5-*a*] pyridine **G-606** (Table 2). The **G-868**/**G-606** comparison and conclusion is representative of the bigger data set of 5-imidazo versus 8-imidazo[1,5-*a*] pyridines. Note that both the 5 and 8-imidazo[1,5-*a*] pyridines inhibit the hERG channel (Table 2).

For the 5-imidazo[1,5-*a*] pyridines we observed poor in vitro/in vivo CL correlation (IV/IV, see Supplemental material) in rat and **G-868** was no exception. Despite efforts to understand the IV/IV disconnect, a satisfactory explanation was elusive and a decision was made to put more weight on in vivo studies in rat. Our qualitative met ID studies indicated **G-868** was stable in rat (82%). Some metabolism occurred on the hydroxamate (10% acid, 5% amide, see Supplemental material; in mouse there is some turnover-NADPH, which appears to be hydrolysis to the acid and accounts for 1.2% of total). Even though our met ID data did not indicate C8 as a site of metabolism, Metasite™[23,24] did (Fig. 4). Thus, **G-879** (HCT116 IC_{50} = 0.14 μM), containing a C8-fluorine was synthesized. From a cell proliferation potency standpoint, the C8 fluorine was not detrimental to potency. However, consistent with the Metasite analysis, C8 fluorine incorporation lowered in vivo CLp, increased half life and oral exposure in rat, consistent with blocking a site of metabolism. Unfortunately CYP2C9 inhibition activity for **G-879** increased sevenfold.

Encouraged it was possible to reduce total and free drug clearance (**G-879** ppb rat = 97%, free drug CL = 55 mL/min/kg vs 1320 mL/min/kg for **G-868**, ppb rat = 99%), increase $T_{1/2}$ and oral exposure by blocking C8, a second Metasite analysis (Fig. 5) indicated that incorporation of a nitrogen at C7 would block metabolism at both C7 and C8 (Fig. 5). Incorporation of a nitrogen at C7 of the imidazo[1,5-*a*] pyridine core was also anticipated to have additional benefits by lowering the *c*log*P*/*c*log*D* and decreasing the pK_a for the imidazo[1,5-*a*] pyrazines. Decreasing lipophilicity

Table 1
Increasing the polarity of the 6,5 heterobicyclic core lowers lipophilicity as reflected in measured log*D* @ pH 7.4

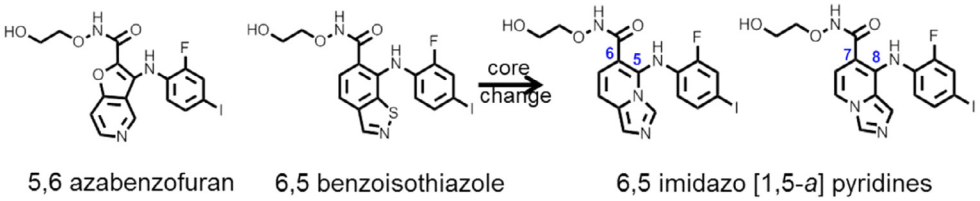

	G-963	G-155	G-868 5-imidazopyridine	G-606 8- imidazopyridine
Cell Proliferation EC_{50} (μM)				
HCT116	0.120	0.044	0.051	0.035
A3750	0.025	0.007	0.004	0.002
clogP	3.1	3.6	2.3	2.3
LogD	3.1	3.1	2.1	2.1
2C9/2C19 IC_{50}(μM)	>10/>10	1.3/1.8	>10/>10	7.3/16
3A4t/m/2D6/1A2 IC_{50}(μM)	>10/>10/>10	9.0/>10/>10	>10/>10/>10	>10/>10/>10

2C9/2C19 cytochrome P450 inhibition is decreased and cell proliferation potency maintained. Target EC_{50} for inhibition of cell proliferation was <0.050 μM (HCT116) and <0.005 μM (A375).

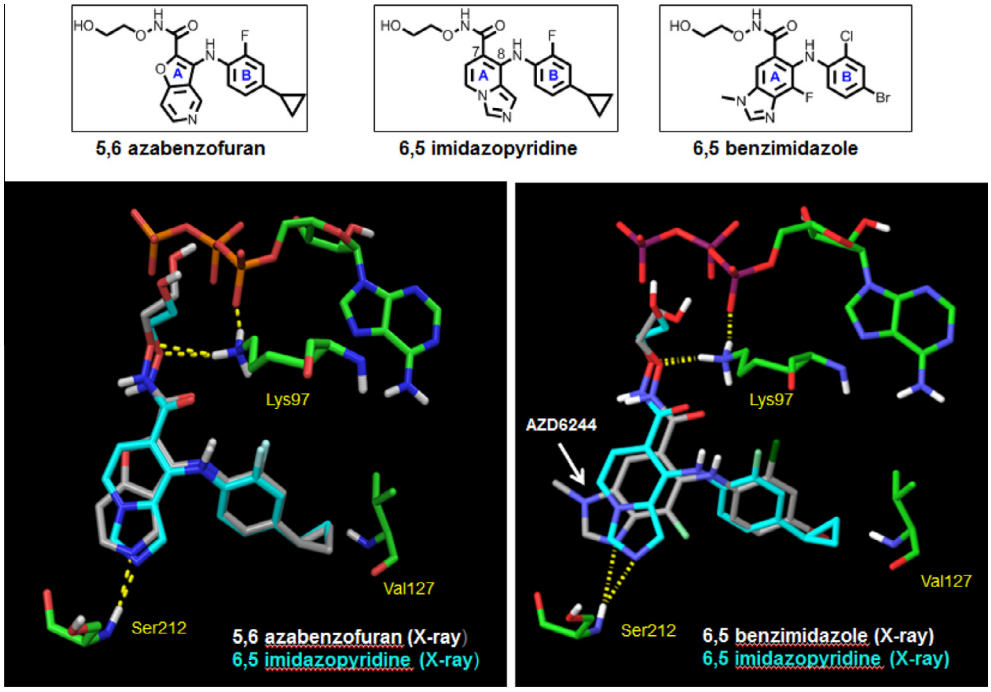

Figure 3. Imidazo[1,5-*a*] pyridine binding mode. Left panel-co-crystal structure of a 5,6 azabenzofuran (2.8 Å resolution; PDB code 4U80) overlayed with a 6,5 imidazopyridine (2.7 Å resolution; PDB code 4U81). The 6,5 imidazopyridine *N* is suitably placed for an H-bond with Ser212 while maintaining the key hydroxamate and anilino pharmacophoric elements in a remarkably similar position as in **G-925**. Right panel-co-crystal structure of a 6,5 benzimidazole (**AZD6244**, 2.8 Å resolution; PDB code 4U7Z) overlayed with the same 6,5 imidazopyridine (PDB code 4U81). It is noteworthy that in the 6,5 imidazopyridine co-crystal structure the attachment point of the five-membered ring heterocycle is shifted towards the B-ring versus its attachment point in **AZD6244**. Despite the shift, the imidazopyridine nitrogen is positioned to make a robust H-bond interaction to the Ser212 while maintaining the key hydroxamate and anilino pharmacophoric elements in a remarkably similar position as in **AZD6244**. These X-ray co-crystal structures support the hypothesis from modelling that novel 6,5 heterobicycles would result in MEKi's that would fit well in the MEK binding pocket and have a high probability for equivalent or improved potency versus the 5,6 azabenzofuran core.

Table 2
Comparative potency, liver microsome stability (H = human, R = rat, M = mouse, D = dog, C = cyno), rat PK and hERG patch clamp IC_{50}'s for **G-868** (representative of the 5-imidazo[1,5-*a*] pyridine class of MEKi') and **G-606** (representative of the 8-imidazo[1,5-*a*] pyridine class of MEKi's)

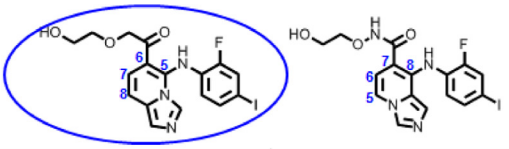

Compound	G-868 5-imidazo[1,5-*a*] pyridine	G-606 8-imidazo[1,5-*a*] pyridine
HCT116 prolif IC_{50}(μM)	0.051	0.035
Mic(H/R/M/D/C)pred.CLhep mL/min/kg	14/38/64/12/30 M/M/H/M/M	15/40/75/23/38 M/M/H/H/H
Rat PK total CL(mL/min/kg), $T_{1/2}$(h), V_{ss}(L/kg), AUC(μM*hr) %F	13.2, 1.7 0.50, 20, >100	14.0, 0.9, 0.46, 6.0, 37
hERG (patch clamp) IC_{50}(μM)	4.4	2.1

IV/PO dose = 1/5 mpk. AUC for **G-868** (IV/PO dose = 1/10 mpk) was normalized to a 5 mpk dose. IV/PO formulations = solution (60%PEG400/40%H_2O)/solution(60%PEG400/40%H_2O) for all compounds dosed. Dose volume = 5 mL/kg for all compounds dosed.
Liver microsomal stability ranges utilized for stable/moderate/labile designations; (CLhep) mL/min/kg; stable (H/R/M) = <6.2:<17:27; moderate (H/R/M) = 6.2–15:17–39:27–63; labile (H/R/M) = >15:>39:>63.

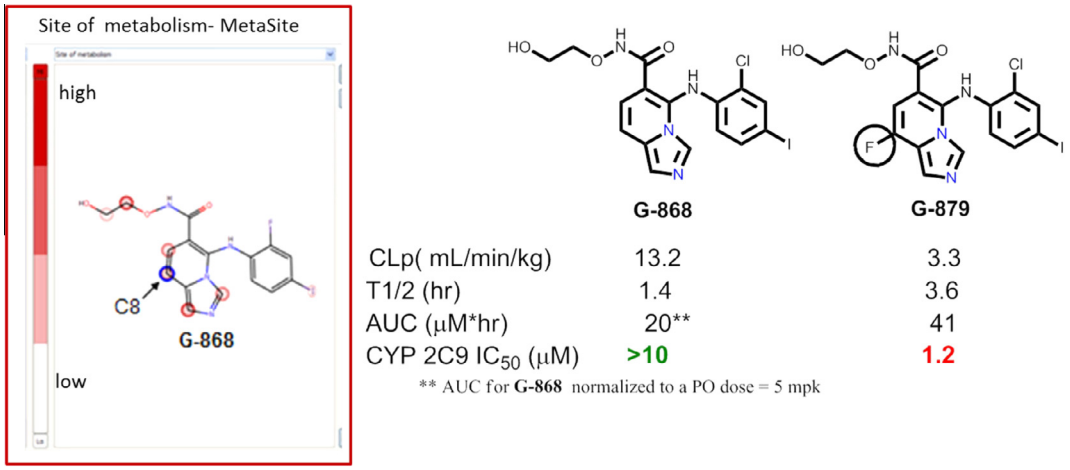

Figure 4. C8 Fluorine substitution improved CLp, $T_{1/2}$, and oral exposure (PO dose 5 mpk, rat) but increased CYP2C9 inhibition activity 7-fold. The more intense the red circle, the higher probability of metabolism (color gradient shown on bar on right and indicates low probability to high probability of metabolism taking place on circled carbon). The major metabolic site is indicated by a blue circle. For **G-868**, the MetaSite software identified C8 as the major metabolic site.

along with decreasing basicity would increase the probability of improving the hERG IC_{50} versus **G-868**. Based on met ID data, the hydroxamate was the major metabolic site of **G-868** and one way to modulate clearance would be to make the hydroxamate less prone to hydrolysis. However, it was difficult to predict a priori how the N7 nitrogen and lower lipophilicity would effect the metabolism of the hydroxamate. **G-593** was synthesized to determine if an imidazo[1,5-*a*] pyrazine could further improve on the imidazo[1,5-*a*] pyridine **G-868** (Fig. 6).

As shown in Table 3, the incorporation of a nitrogen at C7 (**G-593**) lowered the *c*log*P*/*c*log*D* versus **G-868**. Both MOKA and the ACD software predicted a lower pK_a, though the magnitude of decrease is different. The measured pK_a's validated the predictions as the pK_a for **G-593** is two units lower versus **G-868**. However, despite the lower clog*P*/clog*D* and decreased pK_a, there is no change in the hERG IC_{50}. The *measured* log*D* (@ pH 7.4) shows identical values for **G-868 and G-593**, a possible reason for lack of improvement in the hERG IC_{50}. That the overall hydrophobicity, as reflected in log*D* measurements, is identical may reflect "buried" polar surface area in **G-593** if the hydroxamate NH is engaged in an H-bonding interaction with N7. Such an interaction may not be reflected in the log*D*. The working hypothesis that came out of this result was that for the imidazo[1,5-*a*] pyridine MEKi's (Table 3) any improvement in hERG IC_{50} is likely to be driven by decreased lipophilicity (i.e., lowering *measured* log*D*). The imidazole nitrogen in **G-868** is not very basic to begin with (pK_a 4.30), so lowering its pK_a does not impact the hERG IC_{50}.

Though the anticipated improvement in hERG IC_{50} was not realized, further exploration of the imidazo[1,5-*a*] pyrazines was conducted. As shown in Table 4, the cell proliferation potency lost by the addition of a nitrogen at the 7 position could be regained with a more hydrophobic side chain without increasing the log*D* (**G-593** vs **G-327**). **G-593** and **G-327** exhibited higher total CL and lower exposure than **G-868**. However, unlike the imidazo[1,5-*a*] pyridine class of MEKi's, the in vivo clearance was in line with that predicted from in vitro RLM stabilities. The lower total clearance exhibited by **G-868** may be due in part to its high plasma protein binding .*The most pronounced effect of the N7 modification was*

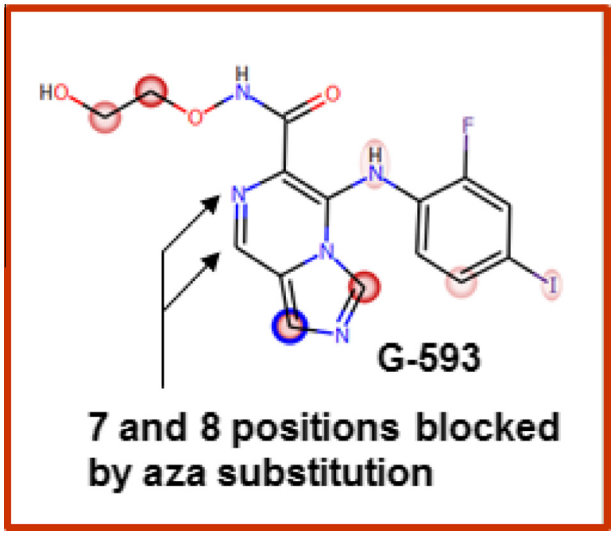

Figure 5. Metasite analysis showing that a nitrogen incorporated at the C7 position removes two potential sites of metabolism. Note the major site of metabolism predicted by MetaSite is now the imidazo ring of the imidazo[1,5-*a*] pyridine core.

decreasing plasma protein binding. Plasma protein binding was decreased across species (3–9%, 7% lower in rat). The nitrogen in **G-593** increased metabolic stability and so lowered the unbound clearance (**G-593** 600 mL/min/kg versus **G-868** 1320 mL/min/kg; ppb (rat) **G-868** = 99%, **G-593** = 92%). Permeability in the A–B direction increased for **G-593** with reduced efflux (B–A/A–B = 0.7 vs 2.60 for **GDC-868**).The improved permeability may be a result of an effective decrease in polar surface area due to the hydroxamate NH engaging in an H-bonding interaction with N7. While such an interaction may not be reflected in the log*D* it could result in improved permeability. Lowering of the plasma protein binding resulting in a lowering of the free drug clearance and improved permeability demonstrated C7 nitrogen modification could influence drug like properties in a positive way.

Encouraged by the improved permeability and the decreased free drug clearance we revisited our working hypothesis that we could improve the hERG IC_{50} by lowering log*D*. It was reasoned that adding a more polar hydroxamate side chain would lower the log*D*. Additionally, spreading polarity throughout the molecule is one strategy that has been utilized to improve hERG by destabilizing the interaction with the lipophilic cavity of the hERG channel.[25] Our microsome stability calculations indicated improvement in

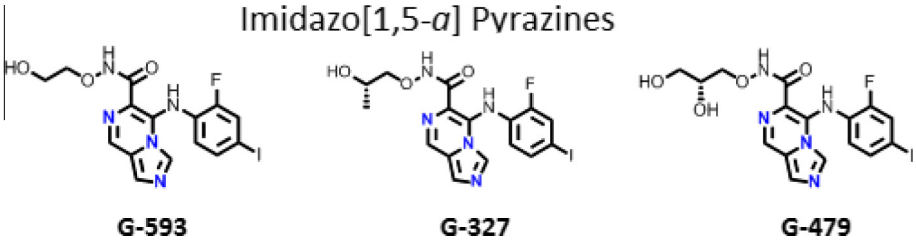

Figure 6. Imidazo[1,5-*a*] pyrazines **G-593**/**G-327**/**G-479**.

Table 3
Comparative cell proliferation potencies, *c*log*D*/*c*log*P*, log*D* @ pH 7.4, calculated and measured pK_a's and hERG patchclamp IC_{50}'s for imidazo[1,5-*a*] pyridine **G-868** and imidazo[1,5-*a*] pyrazine **G-593** Illustrates the value of obtaining measured log *D*'s on a routine basis (RSD for Log *D* = ±0.30)

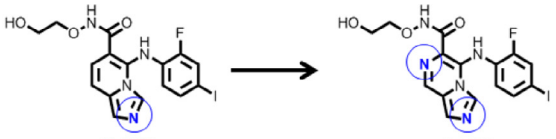

HCT 116 cell prolif IC_{50}(μM)	**0.051**	**0.120**
A375 cell prolif IC_{50}(μM)	**0.004**	**0.008**
clogP/clogD	**2.3/2.3**	**1.6/1.6**
Predicted pKa (MOKA)	**4.78**	**4.35**
Predicted pKa (ACD)	**5.84**	**3.34**
Measured pKa (Sirius)	**4.30**	**2.03**
LogD	**2.1**	**2.1**
hERG patch clamp IC_{50}	**4.4 μM**	**3.3 μM**

For the imidazo[1,5-*a*] pyrazine core, the log *D* may exert a bigger influence on the hERG IC50 than decreasing pK_a.

Table 4
Comparative potency, *c*Log*P*/Log*D*@ pH 7.4, thermodynamic solubility, liver microsome stability, rat PK, MDCK permeability and plasma protein binding (ppb, human, rat, mouse) for novel 6,5-heterobicyclic MEKi's **G-868 and G-606** (imidazo[1,5-*a*] pyridine class), and **G-593**/**G-327**/**G-479** (imidazo[1,5-*a*] pyrazine class). IV/PO dose = 1/5 mpk and 1/10 mpk **G-868**

G# structure	Cell prolif IC_{50} (μM) HCT116/A375	*c*log*P* Log*D*	TS (pH 6.5, μg/mL)	Mic(H/R/M) (mL/min/kg)	PK(rat)CLp/CL(free) (mL/min/kg), F(%), AUC (μM∗h)	MDCK (A–B;B–A; B–A/A–B) 10^{-6} cm/s	ppb (H/R/M) (%)	hERG patch clamp IC_{50} (μM)
G-868 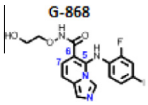	0.049:0.004	2.3 2.05	41(cryst)	14:38:64 M/M/L	13.2:1320 100,20*	6.20:16.5:2.6	99.5:99:94	4.4
G-606 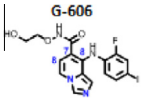	0.035:0.002	2.3 2.05	110 (amorph)	15:40:75 M/M/L	14:636 6,37	20.4:14:0.7	98.5:97.8:95.1	2.1
G-593 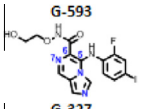	0.120:0.008	1.6 2.10	150 (amorph)	11:41:54 M/L/M	48:600 38,1.48	19.7:14:0.7	91:92:89	3.3
G-327 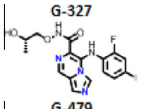	0.052:0.005	2.1 2.2	48 (amorph)	10:44:56 M/L/M	44:800 15,0.61	ND	90:94.5:91	3.3
G-479 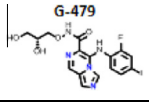	0.107:0.007	0.95 1.1	12 (amorph)	8:19:29 S/M/M	12:92 65,9.2	7.9:8.7:1.3	86:87:87	14

Dose volume = 5 mL/kg for all compounds dosed.
* AUC normalized to a 5 mpk dose for **G-868**. IV/PO formulations = solution (60%PEG400/40%H_2O)/solution (60%PEG400/40%H_2O) for all compounds dosed.

metabolic stability across species with the additional polarity. Incorporation of the diol hydroxamate sidechain in **G-479** lowered the *measured* log*D* and an improvement in the hERG IC_{50} was realized (Table 4). As predicted by in vitro RLM's (the pyrazines exhibited an excellent IV/IV correlation for rat), **G-479** exhibited improved metabolic stability in rat, lower plasma protein binding across species, improved MDCK permeability (less efflux), lower free drug CL (92 mL/min/kg vs 1300 mL/min/kg for **G-868**), and increased LLE (Supplemental material) compared with **G-868**. The in vivo total CLp in rat was equivalent to **G-868**, the exposure and %*F* much improved versus **G-593** and **G-327**. The oral exposure of **G-479** was only two fold lower than that of the lead imidazo[1,5-*a*] pyridine **G-868**. Since the secondary hydroxyl of the diol hydroxamate had no effect on cell proliferation potency (**G-593** 120 nM vs **G-479** 107 nM), the potency loss suffered by **G-479** can be rationalized by a weaker interaction with the Ser212 nitrogen due to the less basic H-bond accepting nitrogen.

The imidazo[1,5-*a*] pyrazines were synthesized by the following 10 step synthetic route (Scheme 1).

Some interesting features of the chemistry included the following:

(a) The reaction did not work at all using LDA obtained from commercial sources. It was necessary to freshly prepare the LDA to obtain **2**. (b) In the conversion of **2** to **3**, if LDA was used as the base it was prepared fresh since that was considered best practice. However, commercial LHDMS (Aldrich) could be used as the base with comparable yields.

(e) In the synthesis of **G-868** the reduction of the nitrile to the benzyl amine was accomplished in good yield by a $CoCl_2$/$NaBH_4$/MeOH reduction.[20,21] Applying the same procedure to **5** gave no product. In the case of pyrazine **5**, the major product isolated from the $CoCl_2$/$NaBH_4$ mediated reduction of **5** was the 2-F 4-TMS aniline. This result necessitated the screening of several reduction conditions to find one that cleanly transformed **5** into **6**. It was found that it was absolutely necessary to run the hydrogenation reaction in glacial acetic acid to achieve a high yield of crude **6** (presumably the acetate salt) which was of suitable purity to be taken on directly. This result also indicated the imidazo[1,5-*a*] pyrazine core is stable under acidic but not basic reaction conditions.

(e)-(h) Crude material was carried through steps (e)-(h) and purification performed on intermediate **9**.

(i) It was necessary to hydrolyze the ester using tin mediated hydrolysis conditions at 85 °C[34] as the more standard hydrolysis conditions of LiOH/THF/MeOH/H_2O resulted in decarboxylation. This result was consistent the previous observation that the imidazo[1,5-*a*] pyrazine core was stable under acidic reaction conditions (even with heating to 85 °C!!) but not basic reaction conditions.

(j) Changing the base from DIPEA to 4-methylmorpholine improved the yield of the coupling reaction 4.5 fold (11–50%).

In planning for success and scalability, there was precedent in the MEK patent literature for hydroxamate formation directly from the ester (74% yield on a 200 g scale).[38] While the imidazo[1,5-*a*] pyrazines were prepared on 50–200 mg scale with the final step being an EDCI/HOBT coupling, we did also explore hydroxamate formation directly from the methyl ester (Scheme 2). When preparing the hydroxamate from the methyl ester, it was critical to use three equivalents of the LHMDS base. Two representative examples are shown below.

A plot of the biochemical potency versus log*D* and *c*log*P* (overall hydrophobicity) can be found in the Supplemental material. Both the LLE versus measured log*D* and calculated *c*Log*P* plots show a progression of the 6,5 heterobicyclic MEKi's towards greater LLE. Imidazo[1,5-*a*] pyrazine **G-479** gained 1.5 units in LLE and is the most ligand efficient 6,5 heterobicycle described in this manuscript.

Leveraging X-ray crystal structure data for **G-925** gave rise to novel 6,5-heterobicyclic cores.[39] The starting point for this work was the novel 6,5 heterobicyclic isobenzothiazole MEKi which interacted with Ser212 in a monodentate fashion as did **G-925** but exhibited increased cell proliferation potency.[1] Unfortunately isobenzothiazole **G-155** was a potent 2C9/2C19 inhibitor which prompted a core change to a more polar 6,5 heterobicyclic core. The imidazo[1,5-*a*] pyridine core with lower lipophilicity

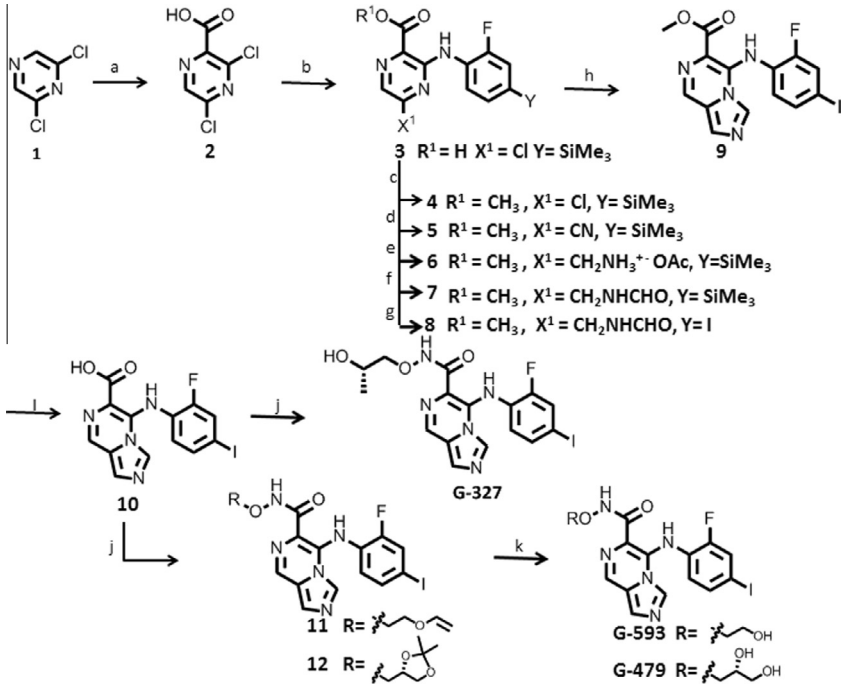

Scheme 1. Reagents and conditions:[26] (a) (i) 1.02 equiv freshly prepared LDA, THF, 1.0 equiv **1**, −78 °C, 2 h; (ii) CO_2 (xs), 41% yield. (b) (i) 2.0 equiv[27] 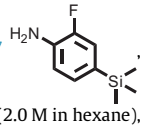 3.0 equiv LHMDS or LDA, THF, −78 °C, 1 h; (ii) 1.0 equiv **2**, THF, −78 °C, 0.5 h to rt, 63% yield. (c) 70% Toluene, 30% MeOH (0.06 M), 0 °C, 2.3 equiv $TMSCHN_2$ (2.0 M in hexane), warm to rt, 1 h, 71% yield, crude pdt. Compound **4** used directly. (d) DMF,[28] 1.0 equiv **4** (0.16 M), 1.1 equiv $Zn(CN)_2$, 0.125 equiv $Pd(PPh_3)$, microwave, 300 W, 150 °C, 25 min, 78% yield. (e) Compound **5**, glacial acetic acid (0.15 M),[29] 10% Pd–C (20% by wt.), H_2 (1 atm, balloon), 1.5 h,[30] 98% yield, crude pdt. Compound **6** used directly. (f) Compound **6**, 75% formic acid/25% acetic anhydride,[31] rt 1.5 h,[32] 80% yield, crude product **7** used directly. (g) Compound **7**, anhydrous DCM (0.1 M), 0 °C, 2.0 equiv iodine monochloride (1.0 M solution in DCM), 0° to rt, 1 h,[33] 98% yield, crude pdt. Compound **8** used directly. (h) Compound **8**, toluene (0.025 M, suspension), 4.2 equiv $POCl_3$, 95 °C, 1 h, SiO_2 purified (ISCO 35–100% EA/hex, followed by 0–30% MeOH/EA) 46% yield. (i) Compound **9**, anhydr. 1,2 DCE (0.14 M), 3.5 equiv $Sn(CH_3)_3OH$, 85 °C, 1 h, 98% yield.[34,35] (j) Compound **10**, anhydr. DMF (0.2 M), 1.04 equiv 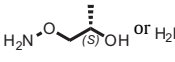 or 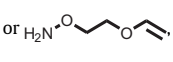 , or 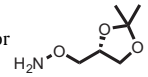 1.05 equiv HOBT, 4.8 equiv 4-methylmorpholine, 1.05 equiv EDCI, rt, 17 h–3 d, 50% yield **G-327**.[36] (k) Anhydrous DCM/MeOH (2:1), 1.5 equiv 4 M HCL in 1,4 dioxane, rt, 1 h; (ii) 6.0 equiv solid $NaHCO_3$, rt, 15 min, then Na_2SO_4 filter and purify on SiO_2 (ISCO, 0–15% MeOH/DCM), 48%, 32% over coupling/deprotection steps **G-593**/**G-479**).[37]

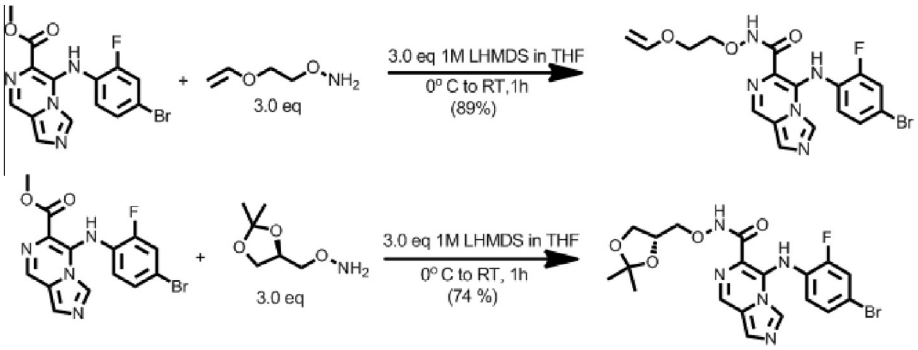

Scheme 2. Preparation of hydroxamate directly from the methyl ester.

eliminated 2C9/2C19 inhibition and increased structural diversity. A new 6,5 heterobicyclic lead emerged, the imidazo[1,5-*a*] pyridine **G-868**.[20] **G-868** went on to become a clinical candidate and was later renamed **GDC-0623**.[19,21] The 6,5-imidazo[1,5-*a*] pyridine scaffold was further optimized by incorporating a nitrogen at the 7 position to yield the 6,5-heterobicyclic imidazo[1,5-*a*] pyrazine core. The introduction of the C7 nitrogen was driven by increasing the structural diversity of the 6,5 heterobicycles while also adding polarity in a position where potency would be retained and metabolic stability improved. Even though in vivo met ID data did not lead us down this road, testing a hypothesis based on a MetaSite prediction resulted in the discovery of a fourth novel and potent 6,5 heterobicyclic scaffold, the imidazo[1,5-*a*] pyrazines. The nitrogen at the 7 position did not result in an improvement in hERG IC_{50} as expected. The learning here was that lowering the lipophilicity (as reflected in lowering the log*D*) is more important for improving hERG than pK_a. The N7 modification did have an effect on physicochemical properties by reducing the plasma protein binding across species. The nitrogen increased metabolic stability and so lowered the unbound clearance. A nitrogen at C7 was not sufficient in itself to improve upon the oral exposure of **G-868** (**GDC-0623**). Combining N7 with a diol hydroxamate which spread the polarity

throughout the molecule gave imidazo[1,5-*a*] pyrazine **G-479** which was improved over **G-868** (**GDC-0623**) in many aspects (e.g., hERG, lower ppb across species, 14× lower free drug CL, improved(H/R/M) microsome stability and passive permeability, Table 4). The LLE analyses done retrospectively (Supplemental material) demonstrates the progression of novel 6,5-heterobicycles towards increased LLE after moving away from the 5,6-aza-benzofuran scaffold.

The core change to the 6,5 heterobicyclic scaffold was potency driven and once discovered further diversified to give additional novel and potent 6,5 heterobicyclic MEKi's. **G-479** did improve on **G-868** (**GDC-0623**) in many aspects but due to the two fold potency loss in HCT116 cell proliferation assay coupled with the two fold lower oral exposure, **G-479** was not able to displace **G-868** (**GDC-0623**) as the development candidate.

This work is yet another example in the medicinal chemistry literature where small structural changes can have big consequences. The 6,5 heterobicycles were enabled by the crystal structure of the 5,6 aza-benzofuran **G-925**.[1] Once the discovery of the first 6,5-heterobicyclic core was made, it offered an opportunity to utilize a successful medicinal chemistry strategy (especially for kinase inhibitors) of incorporating nitrogen atoms in specific places to add polarity, increase structural diversity, improve potency, PK, and properties and give rise to novel MEKi scaffolds. Use of the predictive tool MetaSite was rewarded by the discovery of imidazo[1,5-*a*] pyrazine **G-479.** The design strategy taken was a successful one as demonstrated by the discovery of clinical candidate **GDC-0623** which has progressed to phase 1b.

Acknowledgments

The authors gratefully thank the purification and analytical groups within Genentech Small Molecule Drug Discovery for their support. We also thank Dr Joseph Lyssikatos for helpful discussions and encouragement in making the hydroxamate directly from the methyl ester as described in the patent literature, Dr. Mark Zak for his suggestion to try the trimethyl tin mediated hydrolysis of **9** after the more conventional hydrolysis procedure unexpectedly gave exclusively the decarboxylation product. Dr. Mark Zak and Dr. Anthony Estrada provided helpful discussions on the experimental details of the methyl ester hydrolysis. We acknowledge the use of synchrotron X-ray sources at APS (Advanced Photo Source-Argonne National Laboratory, outside Chicago IL) and SSRL (Stanford Synchrotron Radiation Lightsource, Palo Alto CA) supported by the Department of Energy's (DOE) Office of Science. The SSRL Structural Molecular Biology Program is also supported by DOE's Office of Biological and Environmental Research, and by the National Institutes of Health (NIH). Refinement statistics for the structures in Figure 3 are summarized in the Supplementary material.

Supplementary data

Supplementary data associated with this article can be found, in the online version, at http://dx.doi.org/10.1016/j.bmcl.2014.08.008.

References and notes

1. Heald, R. A.; Jackson, P.; Savy, P.; Jones, M.; Gancia, E.; Burton, B.; Newman, R.; Boggs, J.; Chan, E.; Chan, J.; Choo, E.; Merchant, M.; Rudewicz, P.; Ultsch, M.; Weismann, C.; Yue, Q.; Belvin, M.; Price, S. *J. Med. Chem.* **2012**, *55*, 4594. A reading of Ref. [1] is recommended for key background information, the genesis of the 5,6 scaffolds and the origin and significance of isobenzothiazole **G-155** which is used as the starting point for the **G-479** discovery..
2. Downward, J. *Nat. Rev. Cancer* **2003**, *3*, 11.
3. Bamford, S.; Dawson, E.; Forbes, S.; Clements, J.; Pettett, R.; Dogan, A.; Flanagan, A.; Teague, J.; Futreal, P. A.; Stratton, M. R.; Wooster, R. *Br. J. Cancer* **2004**, *91*, 355.
4. Hoshino, R.; Chantani, Y.; Yamori, T.; Tsuruo, T.; Oka, H.; Yoshida, O.; Shimada, Y.; Ari-I, S.; Wada, H.; Fujimoto, J.; Kohno, M. *Oncogene* **1999**, *18*, 813.
5. Hatzivassiliou, G.; Song, K.; Yen, I.; Brandhuber, B. J.; Anderson, D. J.; Alvarado, R.; Ludlam, M. J.; Stokoe, D.; Gloor, S. L.; Vigers, G.; Morales, T.; Aliagas, I.; Liu, B.; Sideris, S.; Hoeflich, K. P.; Jaiswal, B. S.; Seshagiri, S.; Koeppen, H.; Belvin, M.; Friedman, L. S.; Malek, S. *Nature* **2010**, *464*, 431.
6. Heidorn, S. J.; Milagre, C.; Whittaker, S.; Nourry, A.; Niculescu-Divas, I.; Dhomen, N.; Hussain, J.; Reis-Filo, J. S.; Springer, C. J.; Pritchard, C.; Marais, R. *Cell* **2010**, *140*, 209.
7. Poulikakos, P. I.; Zhang, C.; Bollag, G.; Shokat, K. M.; Rosen, N. *Nature* **2010**, *464*, 427.
8. Solit, D. B.; Garraway, L. A.; Pratilas, C. A.; Sawai, A.; Getz, G.; Basso, A.; Ye, Q.; Lobo, J. M.; She, Y.; Osman, I.; Golub, T. R.; Sebolt-Leopold, J.; Sellers, W. R.; Rosen, N. *Nature* **2006**, *439*, 358.
9. Wellbrock, C.; Karasarides, M.; Marais, R. *Nat. Rev. Mol. Cell Biol.* **2004**, *5*, 875.
10. Flaherty, K. T.; Infante, J. R.; Daud, A.; Gonzalez, R.; Kefford, R. F.; Sosman, J.; Hamid, O.; Schuchter, L.; Cebon, J.; Ibrahim, N.; Kaduchadkar, R.; Burris, H. A., III; Falchook, G.; Algazi, A.; Lewis, K.; Long, G. V.; Puzanov, I.; Lebowitz, P.; Singh, A.; Little, S.; Sung, P.; Allred, A.; Ouellet, D.; Kim, K. B.; Patel, K.; Weber, J. *N. Eng. J. Med.* **2012**, *367*, 1694.
11. Clinical Trials.gov NCT01138085 Safety, PK of AKT and MEK Combination (GSK1120212 and GSK2141795) Currently recruiting patients.
12. Haagensen, E. J.; Kyle, S.; Beale, G. S.; Maxwell, R. J.; Newell, D. R. *Br. J. Cancer* **2012**, *106*, 1386.
13. Shimizu, T.; Tolcher, A. W.; Papadopoulos, K. P.; Beeram, M.; Rasco, D. W.; Smith, L. S.; Gunn, S.; Smetzer, L.; Mays, T. A.; Kaiser, B.; Wick, M. J.; Alvarez, C.; Cavazos, A.; Mangold, G. L.; Paitnaik, A. *Clin. Cancer Res.* **2012**, *18*, 2316.
14. Menzies, A. M.; Long, G. V. *Ther. Adv. Med. Oncol.* **2013**, *5*, 278.
15. Wagle, N.; Van Allen, E. M.; Treacy, D. J.; Frederick, D. T.; Cooper, Z. A.; Taylor-Weiner, A.; Rosenberg, M.; Goetz, E. M.; Sullivan, R. J.; Farlow, D. N.; Friedrich, D. C.; Anderka, K.; Perrin, D.; Johannessen, C. M.; McKenna, A.; Cibulskis, K.; Kryukov, G.; Hodis, E.; Lawrence, D. P.; Fisher, S.; Getz, G.; Gabriel, S. B.; Carter, S. L.; Flaherty, K. T.; Wargo, J. A.; Garraway, L. A. *Cancer Discov.* **2014**, *4*, 61.
16. Price, S. *Expert Opin. Ther. Pat.* **2008**, *18*, 603.
17. Ohren, J. F.; Chen, H.; Pavlovsky, A.; Whitehead, C.; Zhang, E.; Kuffa, P.; Yan, C.; McConnell, P.; Spessard, C.; Banotai, C.; Mueller, W. T.; Delaney, A.; Omer, C.; Sebolt-Leopold, J. S.; Dudley, D. T.; Leung, I. K.; Flamme, C.; Warmus, J.; Kaufman, M.; Barrett, S.; Tecle, H.; Hasemann, C. A. *Nat. Struct. Mol. Biol.* **2004**, *11*, 1192.
18. Fischmann, T. O.; Smith, C. K.; Mayhood, T. W.; Myers, J. E., Jr.; Reichert, P.; Mannarino, A.; Carr, D.; Zhu, H.; Wong, J.; Yang, R.; Le, H. V.; Madison, V. S. *Biochemistry* **2009**, *48*, 2661.
19. Hatzivassiliou, G.; Haling, J. R.; Chen, H.; Song, K.; Price, S.; Heald, R.; Hewitt, J. F. M.; Zak, M.; Peck, A.; Orr, C.; Merchant, M.; Hoeflich, K. P.; Chan, J.; Luoh, S.-M.; Anderson, D. J.; Ludlam, M. J. C.; Wiesmann, C.; Ultsch, M.; Friedman, L. S.; Malek, S.; Belvin, M. *Nature* **2013**, *501*, 232.
20. **G-868** appeared in the patent literature in 2009: Price, S.; Heald, R.; Lee, W.; Zak, M. E.; Hewitt, J.; Frances M. WO 85983 A1, 2009.
21. For the first public disclosure of the structure of **GDC-0623**, see Supplemental material in Ref. [19].
22. **G-606** appeared in the patent literature in 2009: Price, S.; Heald, R.; Savy, P. P. A. WO 85980 A1, 2009.
23. Caron, G.; Ermondi, G.; Testa, B. *Pharm. Res.* **2007**, *24*, 480.
24. See also http://www.moldiscovery.com/publications.php MetaSite.
25. Jamieson, C.; Moir, E. M.; Rankovic, Z.; Wishart, G. *J. Med. Chem.* **2006**, *49*, 5029.
26. All reactions except (e) were run in oven dried glassware cooled under N_2, under an atmosphere of N_2. Reagents were used as received from commercial sources without any additional purification.
27. The preparation of 2-fluoro-4-(trimethylsilyl)aniline, was first disclosed in: Goutopolis, A.; Askew, Jr., B. C.; Chen, X.; Srinivasa, K.; Yu, H. WO123936 A1, 2007. See also Price, S.; Heald, R.; Lee, W.; Zak, M. E.; Hewitt, J.; Frances M. WO 85983 A1, 2009; WO3025A1, 2010; WO3022A1, 2010; WO93013A1, 2009.
28. A fresh bottle of anhydrous DMF was degassed by sparging with nitrogen for 2 h prior to the running of the cyanation reaction.
29. Prior to adding the 10% Pd–C catalyst, the round bottomed flask was evacuated under house vacuum and filled with nitrogen 3×.
30. Reaction times longer than 1.5 h (i.e., 3 h) resulted in over-reduction products being formed.
31. Concd = 0.16 M, and a suspension resulted. The reaction mixture to form (**7**) never became homogeneous.
32. After extractive workup (EtOAc, satd $NaHCO_3$/water/brine wash, Na_2SO_4 drying), crude pdt. (**7**) was azeotroped with DCM to give an orange foam of suitable purity by LC/MS to be used directly without purification for the next step.
33. After extractive workup (EtOAc, satd $NaHCO_3$/water/brine wash, Na_2SO_4 drying), crude pdt. (**8**) was azeotroped with DCM to give a yellow sold of suitable purity to be carried on directly to the next step.
34. Nicolaou, K. C.; Zak, M.; Safina, B. S.; Estrada, A. A.; Lee, S. H.; Nevalainen, M. *J. Am. Chem. Soc.* **2005**, *127*, 11176.
35. After extractive workup (EtOAc, 1 M HCl (3×)/water/brine wash, Na_2SO_4 drying), the crude product (**10**) was treated with DCM/Et_2O/hexane. Crystals resulted which were collected by suction filtration and dried under house vacuum and used in the hydroxamate coupling reactions.
36. Crude **G-327** was purified by SiO_2 chromatography (ISCO, 65–100% EA/hex, followed by 0–50% MeOH/EA) and the resulting viscous oil treated with DCM (1 drop)/ether/hexane to afford a yellow solid. The ether/hexane/DCM solution

from which the yellow solid precipitated was removed from the round bottomed flask via pipette, transferred to a second round bottomed flask and concentrated. The resulting oil was purified by prep HPLC to give additional **G-327** of >98% purity. The yellow solid that had precipitated after treatment with DCM (1 drop)/ether/hexane precipitate was dried under high vacuum overnight.

37. Crude hydroxamate was purified by SiO_2 chromatography (ISCO, 0–10% MeOH/DCM). **G-573** and **G-479** were crystallized from DCM/ether/hexane. Collected yellow solid via filtration and dried under high vacuum overnight.
38. Marlow, A. L.; Wallace, E.; Seo, J.; Lyssikatos, J. P.; Yang, H. W.; Blake, J.; Storey, R. A.; Booth, R. J.; Pittam, J. D.; Leonard, J. et al. WO044084 A2 20070419, 2007.
39. Heald, R. A.; Jackson, P.; Lyssikatos, J.; Price, Stephen; Savy, P. P. WO2010/3025A1, 2010.